ACS OMEGA

http://pubs.acs.org/journal/acsodf

Article

Numerical Analysis of Soil Deformation and Collapse Due to Hydrate Decomposition

Lele Yang, Jing Wang, Yongliang Yang, and Guangrui Sun*

Cite This: *ACS Omega* 2021, 6, 5335−5347

Read Online

ACCESS | Metrics & More | Article Recommendations

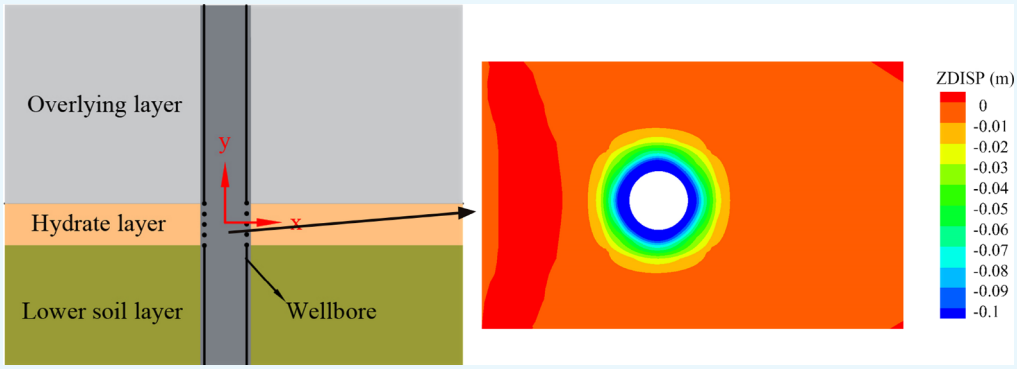

ABSTRACT: Natural gas hydrates are an ideal alternative clean energy source. Many countries are currently attempting the trial production of gas hydrates. Japan became the first country to achieve offshore hydrate trial production in 2013, and China conducted 60 days of continuous trial exploitation in 2017. This study analyzes the changes in the internal stress of the hydrate zone and hydrate saturation of the soil throughout the monitoring period and calculates the failure stress of the hydrate deposit layer. The Mohr−Coulomb model is used to simulate Japan's test exploitation conditions to verify the feasibility of the method. Finally, the hydrate decomposition range, the difference in the soil dip angle in the test exploitation area, and the bearing capacity of the hydrate reservoir are numerically simulated to evaluate the stability of the soil. Through the sensitivity analysis of the hydrate decomposition range and the inclination angle of the hydrate sediment layer, it can be found that the hydrate decomposition range has the greatest impact on the deformation, and the soil around the decomposition area may be sheared and collapsed. Within 1 week of decompression and exploitation, the hydrate decomposition radius is approximately 3 m. When the inclination angle increases from 3° to 9°, the sediment deformation increases by 12 times. Therefore, it is necessary to pay attention to the critical value of the decomposition range during the exploitation process.

1. INTRODUCTION

Natural gas hydrates are cage-like, crystalline solids in which a hydrocarbon, commonly methane, is trapped in an ice lattice. Hydrates are formed under high pressure and low temperature[1−4] and are mainly deposited in the sediments of the deep-water continental slope or buried in polar regions.[5] The stability of hydrates in the environment depends on the surrounding temperature, pressure, and gas source.[6] The changes in pressure and temperature in a longer distance especially in pipeline systems are more favorable conditions for hydrate formation.[7] The amount of conventional energy stored worldwide is limited and will soon be exhausted. As hydrates are widely distributed on land and in the sea,[8] the demand for a potential clean energy source[9−11] can be fulfilled.

The current methods for producing hydrates include thermal excitation,[12−14] pressure reduction,[15] hydrate inhibition,[12,13] and carbon dioxide replacement.[16] As hydrates have been extensively surveyed worldwide, several countries have conducted trial exploitation.[17] In 2013, Japan conducted a test to verify the feasibility of depressurization to extract offshore methane hydrate.[18−20] Although the development and utilization of hydrates can meet the energy demand, the environmental and geological disasters caused by exploitation must be considered.[21,22] First, the possible risks involved, such as methane leakage and land subsidence, must be evaluated,[23−26] followed by conducting reliable risk assessments and responding accordingly.

Received: November 9, 2020
Accepted: February 10, 2021
Published: February 18, 2021

https://dx.doi.org/10.1021/acsomega.0c05463
ACS Omega 2021, 6, 5335−5347

The decomposition of hydrates can lead to large-scale ocean floor collapse. Soil collapse in parts of the United States east coast continental slope, through field detection, is most likely the collapse of the overlying soil layer of the hydrate reservoir.[27] There are two main reasons for the instability of the seabed caused by hydrates. One is the loss of strength of the hydrate itself because of dissociation,[28] in which the state of hydrate changed from solid to liquid and gas. The phase change causes weakness in the formation. The other is the rise in excess pore pressure and loss of effective stress when the hydrate dissociates.[29] The hydrate layer is a poorly stable layer of sediment that has not formed into rocks.[30] Moreover, changes in the weather and sea level may cause the hydrate to decompose and generate additional free gas, which can potentially increase the pore pressure of the hydrate sediment layer and decrease the stability of the storage layer, thereby causing geological disasters, such as landslides.[23−26,31] During the hydrate dissociation, the hydrate layer softens and the pore fluid pressure exceeds the total stress of the overlying layer, leading to the formation of layered fracture between the hydrate layer and the overlying layer.[32] To date, most international research studies have focused on large-scale submarine landslides and the stability of large-scale submarine slopes.[33] The depressurization process used for gas extraction significantly changes the stress state and the mechanical properties of hydrate soils, which may lead to potential geotechnical hazards such as submarine landslide.[34] Detailed theoretical analysis of submarine landslide events caused by hydrate decomposition has been conducted, and the effects of seawater depth, overburden thickness, and hydrate content on slope stability have been analyzed in detail. Additionally, the possible reasons for the instability of hydrates have been described, the triggering mechanism of the three major hydrates has been summarized, and mechanical slope stability models have been analyzed. In Japan, methane production and soil deformation to destruction during hydrate exploitation were simulated by considering the relevant physical mechanisms and conducting theoretical analysis and numerical simulation of the geological conditions of the test site in 2013.[18,35] Combined with physical effects, such as hydrate phase transition, fluid flow, and heat transfer, the possible geological disasters caused by hydrate decomposition were analyzed.[36] However, because the analysis conducted in Japan was based on the specific geological conditions observed during the trial exploitation period, the findings cannot be considered universal. Furthermore, less attention was given to local soil deformation. Therefore, it is clear that the main focus of research on hydrates is their exploration and development. While some studies have focused on the natural disasters caused by hydrate decomposition as well, a few studies have been conducted on instability. Most studies have focused on a wide range of submarine landslides. Although theoretical analysis of local soil instability has been conducted, no specific numerical simulations have been performed to discuss the deformation and failure laws.

It can be seen from previous studies and some on-site trial exploitation that with the continuous trial exploitation, the hydrate decomposition range gradually increases, resulting in a sharp increase in the possibility of large deformation of the overlying soil. To ensure the safety of the hydrate exploitation process, it is necessary to conduct exploration and simulation research in advance for exploitation at different locations to ensure the stability of the exploitation site. In this study, followed by theoretical analysis, MATLAB is used to determine the sensitive parameters, and FLAC3D is used for numerical simulation. Gas hydrate reservoir simulators help provide these assurances not only by forecasting long-term production rates of gas from methane gas hydrate reservoirs but also by predicting the reservoir's mechanical behavior.[37] All the parameters employed in the simulation used the actual measurement data of the test site.[38] Furthermore, a preliminary assessment of the safety of hydrate trial exploitation is conducted, considering the gradual increase in the decomposition range of hydrates over time, different hydrate deposit dip angles and physical properties, and the deformation of the soil layer around the wellbore.

2. VERIFICATION OF THE NUMERICAL MODEL

At present, recreating large-scale working conditions in laboratories is challenging. During the 2013 trial exploitation in Japan, numerical simulation was employed to predict the possible trial exploitation conditions and their safety. Moreover, the safety of the trial exploitation process was evaluated. Since numerically simulating hydrate production is an economically viable method, based on the trial exploitation conducted in Japan, in this study, numerical simulation is used to evaluate the safety of the working conditions.

2.1. The Basic Principle of Adopting the Model. FLAC3D uses the finite difference method for analysis, that is, the fast Lagrangian finite difference calculation program, which can better simulate the force characteristics of the soil, reaching the failure limit. In the soil mechanics method, the failure envelope of the Mohr−Coulomb model mainly includes two parts: the shear failure envelope and the tensile failure envelope. Corresponding to the shear failure is an associated flow law, and the tensile failure corresponds to an uncorrelated flow law. Combining the incremental model of plasticity theory and the Mohr−Coulomb criterion and tensile failure criterion, the Mohr−Coulomb model used in FLAC3D is formed to better perform the elastoplastic analysis of soil.

In this study, the Mohr−Coulomb model is used to simulate the trial exploitation conditions in Japan. First, the constitutive relationship of Mohr−Coulomb model is introduced. The model can produce two parts of elastic and plastic deformation, which are expressed in the principal stress space of σ_1, σ_2, σ_3, and the corresponding strain component is the principal strain ε_1, ε_2, ε_3. According to Hooke's law, the relationship between stress and strain is $\Delta[\sigma] = [E]\Delta[\varepsilon]$, where $[E]$ is the stiffness matrix.

In the principal stress space, the stress increment can be determined by the following formula.[39]

$$\begin{aligned}\Delta\sigma_1 &= \alpha_1\Delta\varepsilon_1^e + \alpha_2(\Delta\varepsilon_2^e + \Delta\varepsilon_3^e)\\ \Delta\sigma_2 &= \alpha_1\Delta\varepsilon_2^e + \alpha_2(\Delta\varepsilon_1^e + \Delta\varepsilon_3^e)\\ \Delta\sigma_3 &= \alpha_1\Delta\varepsilon_3^e + \alpha_2(\Delta\varepsilon_1^e + \Delta\varepsilon_2^e)\end{aligned} \quad (1)$$

where α_1 and α_2 can be obtained from the shear modulus and bulk modulus.

$$\begin{aligned}\alpha_1 &= K + \frac{4}{3}G\\ \alpha_2 &= K - \frac{2}{3}G\end{aligned} \quad (2)$$

Equation 1 can also be written as follows

https://dx.doi.org/10.1021/acsomega.0c05463
ACS Omega 2021, 6, 5335−5347

$$S_1(\Delta\varepsilon_1^e, \Delta\varepsilon_2^e, \Delta\varepsilon_3^e) = \alpha_1\Delta\varepsilon_1^e + \alpha_2(\Delta\varepsilon_2^e + \Delta\varepsilon_3^e)$$
$$S_2(\Delta\varepsilon_1^e, \Delta\varepsilon_2^e, \Delta\varepsilon_3^e) = \alpha_1\Delta\varepsilon_2^e + \alpha_2(\Delta\varepsilon_1^e + \Delta\varepsilon_3^e)$$
$$S_3(\Delta\varepsilon_1^e, \Delta\varepsilon_2^e, \Delta\varepsilon_3^e) = \alpha_1\Delta\varepsilon_3^e + \alpha_2(\Delta\varepsilon_1^e + \Delta\varepsilon_2^e) \quad (3)$$

The Mohr−Coulomb model uses the Mohr−Coulomb criterion and the maximum tensile stress criterion. If the three principal stresses are $\sigma_1 \le \sigma_2 \le \sigma_3$, then the failure criterion has the form $f^s = 0$, where

$$f^s = \sigma_1 - \sigma_3 N_\phi + 2c\sqrt{N_\phi} \quad (4)$$

For tensile damage, $f^t = 0$, where

$$f_t = \sigma_3 - \sigma^t \quad (5)$$

In eqs 4 and 5, ϕ> is the internal friction angle, c is the cohesive force, and σ^t is the tensile strength.[39]

$$N_\phi = \frac{1 + \sin(\phi)}{1 - \sin(\phi)} \quad (6)$$

The value of the compressive strength σ^t of the material cannot exceed σ_3. The maximum value of σ^t can be expressed as follows.

$$\sigma^t_{\max} = \frac{c}{tg(\phi)} \quad (7)$$

For the plastic flow state, g^s and g^t are the functional relationships corresponding to shear failure and tensile failure, respectively, which are expressed as follows

$$g^s = \sigma_1 - \sigma_3 N_\psi \quad (8)$$

$$g_t = \sigma_3 \quad (9)$$

where ψ is the expansion angle.

$$N_\psi = \frac{1 + \sin(\psi)}{1 - \sin(\psi)} \quad (10)$$

The flow criterion can be defined as a functional relationship $h(\sigma_1, \sigma_3) = 0$, and the parts above $f^s = 0$ and $f^t = 0$ are divided into two regions in the σ_1 and σ_3 planes. The function expression is as follows

$$h = \sigma_3 - \sigma^t + a^P(\sigma_1 - \sigma^P) \quad (11)$$

where a^P and σ^P are defined by the following formula

$$a^P = \sqrt{1 + N_\phi^2} + N_\phi$$
$$\sigma^P = \sigma^t N_\phi - 2c\sqrt{N_\phi} \quad (12)$$

Shear failure occurs when the stress state satisfies $f^s < 0$ and $h < 0$. However, tensile failure occurs when $f^s > 0$ and $h > 0$ are satisfied.

For shear failure, the following formula is obtained from eq 8.

$$\frac{\partial g^s}{\partial \sigma_1} = 1$$
$$\frac{\partial g^s}{\partial \sigma_2} = 0$$
$$\frac{\partial g^s}{\partial \sigma_3} = -N_\psi \quad (13)$$

Substituting $\Delta\varepsilon_1^e$, $\Delta\varepsilon_2^e$, and $\Delta\varepsilon_3^e$in eq 3 with $\frac{\partial g^s}{\partial \sigma_1}$, $\frac{\partial g^s}{\partial \sigma_2}$, and $\frac{\partial g^s}{\partial \sigma_3}$, respectively, gives the following equation.

$$S_1\left(\frac{\partial g^s}{\partial \sigma_1}, \frac{\partial g^s}{\partial \sigma_2}, \frac{\partial g^s}{\partial \sigma_3}\right) = \alpha_1 - \alpha_2 N_\psi$$
$$S_2\left(\frac{\partial g^s}{\partial \sigma_1}, \frac{\partial g^s}{\partial \sigma_2}, \frac{\partial g^s}{\partial \sigma_3}\right) = \alpha_2(1 - N_\psi)$$
$$S_3\left(\frac{\partial g^s}{\partial \sigma_1}, \frac{\partial g^s}{\partial \sigma_2}, \frac{\partial g^s}{\partial \sigma_3}\right) = -\alpha_1 N_\psi + \alpha_2 \quad (14)$$

From eq 4, the following equation can be obtained using $f = f^s$.

$$\sigma_1^N = \sigma_1^I - \frac{f^s(\sigma_1^I, \sigma_3^I)}{(\alpha_1 - \alpha_2 N_\psi) - (-\alpha_1 N_\psi + \alpha_2)N_\phi}(\alpha_1 - \alpha_2 N_\psi)$$
$$\sigma_2^N = \sigma_2^I - \frac{f^s(\sigma_1^I, \sigma_3^I)}{(\alpha_1 - \alpha_2 N_\psi) - (-\alpha_1 N_\psi + \alpha_2)N_\phi}\alpha_2(1 - N_\psi)$$
$$\sigma_3^N = \sigma_3^I - \frac{f^s(\sigma_1^I, \sigma_3^I)}{(\alpha_1 - \alpha_2 N_\psi) - (-\alpha_1 N_\psi + \alpha_2)N_\phi}(-\alpha_1 N_\psi + \alpha_2) \quad (15)$$

Considering the case of tensile failure, the following equation can be obtained using similar methods employed for shear failure.

$$\sigma_1^N = \sigma_1^I - (\sigma_3^I - \sigma^t)\frac{\alpha_2}{\alpha_1}$$
$$\sigma_2^N = \sigma_2^I - (\sigma_3^I - \sigma^t)\frac{\alpha_2}{\alpha_1}$$
$$\sigma_3^N = \sigma^t \quad (16)$$

When using the Mohr−Coulomb model, the stress increment calculated by Hooke's law is superimposed on the original stress calculation (σ_{ij}^I), during which the principal stress can be calculated. If the principal stress reaches the failure criterion, then two failure situations take place. In the first case, shear failure occurs and σ_1^N, σ_2^N, $\sigma_3^N$is obtained from eq 15. In the second case, tensile failure occurs and σ_1^N, σ_2^N, $\sigma_3^N$is obtained from eq 16.

The Mohr−Coulomb model is a constitutive model of elastoplastic soil, which mainly studies the tensile and shear failure of soil. In this study, the hydrate system is simplified and analyzed without considering the hydrate decomposition process. This paper temporarily ignores the seepage during

https://dx.doi.org/10.1021/acsomega.0c05463
ACS Omega 2021, 6, 5335−5347

the hydrate decomposition process. Some parameters of soil mechanical properties such as the internal friction angle, elastic modulus, Poisson's ratio, and cohesion force are relatively important. This is because the physical problem studied in this paper is mainly the change rule of the displacement of the overlying soil. When the hydrate is completely decomposed, the soil softens, the bearing capacity decreases, and the mechanical parameters of the hydrate layer change, resulting in the deformation of the overlying soil layer. The following two states are mainly studied. One is that the soil in the hydrate trial exploitation area is completely hollowed out and cannot bear any pressure. The second is that the soil in the hydrate trial exploitation area is deformed due to the decomposition of hydrate and the mechanical properties of the soil are weakened. Through the study of these two situations, it is roughly estimated how long the trial exploitation will take before the soil collapse.

2.2. Japanese Trial Exploitation. In 2013, Japan followed the antipressure method to conduct the first near-seawater trial worldwide.[40] Figure 1 shows the plane strain model used for

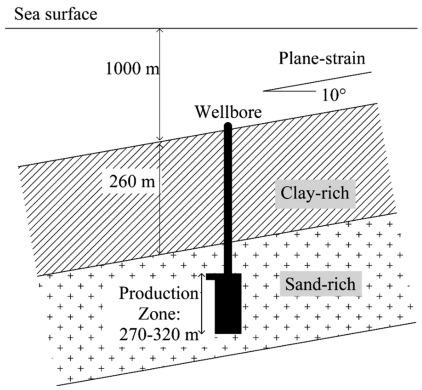

Figure 1. Trial exploitation model for the Japanese numerical simulation. Reprinted with permission from the work of Zhou et al.[41] Copyright 2014 Offshore Technology Conference.

numerical simulation before the trial exploitation, consisting of a seafloor that is assumed to be 1000 m below the sea level and slope angle to be 10°, which simplifies the three-dimensional problem into a two-dimensional problem. The model also assumed that hydrate is only present in the sand-rich layer, and the boundary between the clay- and sand-rich layers is set at 260 m below the seabed. The clay-rich layer has a density of 1750 kg/m^3, cohesive force of 35 kPa, internal friction angle of 15°, elastic modulus of 14 MPa, and Poisson's ratio of 0.2. Meanwhile, the sand-rich layer has a density of 1900 kg/m^3, cohesive force of 2 kPa, internal friction angle of 32°, elastic modulus of 34 MPa, and Poisson's ratio of 0.3.

The Japanese simulation results indicate that hydrate decomposition reduces the strength of the formation, increasing its plasticity.[41] When the local layer reaches the critical plastic deformation state, the volumetric strain increases. The sediment sinks due to the decomposition of the hydrate, and the largest vertical displacement occurs at the interface between the sand and clay layers (Figure 2a). Owing to the decrease in the effective stress, the sediment undergoes compression deformation and is displaced horizontally (Figure 2b).

2.3. Comparative Analysis of the Simulation Results. In this paper, the hydrate system is simplified and analyzed without considering the hydrate decomposition process. The deformation of the overlying soil layer in the following two states is mainly studied. One is that the soil in the hydrate trial exploitation area is completely hollowed out and cannot bear any pressure. The second is that the soil in the hydrate trial exploitation area is deformed due to the decomposition of hydrate and the mechanical properties of the soil are weakened. Through the study of these two situations, it is roughly estimated how long the trial exploitation will take before the soil collapse. The elastic and Mohr−Coulomb models in FLAC3D are used to simulate the trial exploitation conditions in Japan, and the influence of the boundary effect on the simulation is considered. As the model is symmetrical, Figure 3 shows a two-dimensional plan view. Both the length

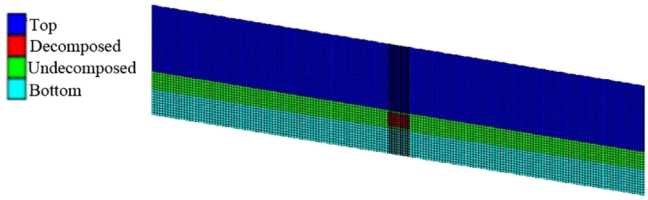

Figure 3. Diagram of the numerical model.

and width of the model are 1800 m, the height is 430 m, and the inclination is 10°. From top to bottom, the structure of the soil is divided into overlying, hydrate, and lower layers. The thicknesses of the overlying, hydrate, and lower layers are 260, 70, and 100 m, respectively, and the sea depth is 1000 m. The wellbore used at 900 m is placed at the center of the model. According to the trial exploitation conducted by Japan, the hydrate decomposition zone forms a cylinder, with a radius of 40 m and a height of 50 m, along the wellbore. The grid size and area of the hydrate decomposition zone are 4 and 10 m, respectively. For the boundary conditions of the model, the two ends of the model in the normal direction are fixed, and the lateral boundary is fixed to limit the lateral displacement.

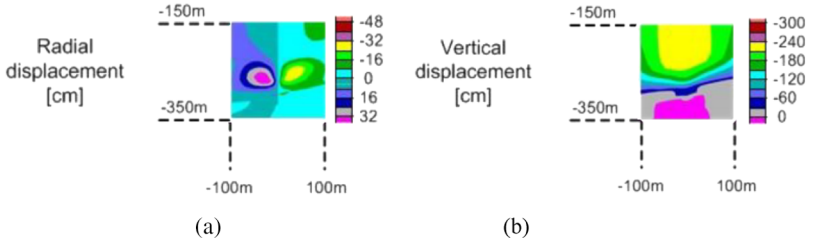

Figure 2. Simulated displacement contours for the Japanese trial: (a) horizontal displacement and (b) vertical displacement. Reprinted with permission from the work of Zhou et al.[41] Copyright 2014 Offshore Technology Conference.

https://dx.doi.org/10.1021/acsomega.0c05463
ACS Omega 2021, 6, 5335−5347

Additionally, the bottom is fixed to ensure that it does not displace vertically. The upper slope is the only free surface.

The comparison between Figures 2 and 4 is shown in Table 1. It can be seen that the variation trends of the soil for the two

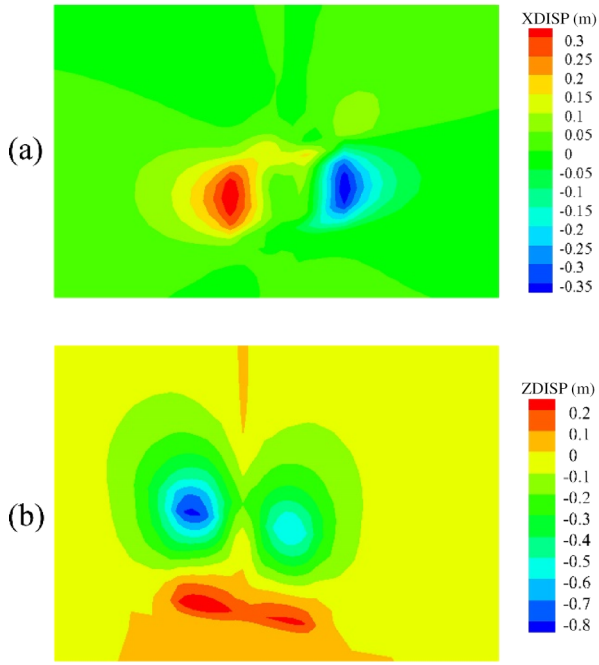

Figure 4. Displacement contours: (a) horizontal displacement and (b) vertical displacement.

Table 1. Comparison of the Simulation Results of This Study and the Japanese Study

	vertical displacement	radial displacement
Japanese study	0.09 m	0.048 m
this study	0.083 m	0.04 m
relative error	0.007 m	0.008 m
error ratio	7.78%	16.67%

simulated working conditions are basically the same. The maximum vertical and horizontal displacements in the Japanese study are approximately 0.09 and 0.048 m, respectively; moreover, the horizontal displacement is toward the center. However, in this study, the maximum vertical and horizontal displacements are approximately 0.083 (Figure 4a) and 0.04 m, respectively, with the horizontal displacement toward the center (Figure 4b).

The simulation results of this study are consistent with the results of the Japanese trial exploitation. The hydrates studied in this paper are stored in the deep seas. The hydrates studied during the trial exploitation in Japan are also stored in the deep sea. The geological structure is basically the same. Japan is mainly composed of overlying sandy soil, and the offshore waters of China are mainly composed of clay. In the model, the difference between sand and clay is mainly reflected in the different mechanical characteristics of the soil. Therefore, the numerical model developed in this study is adequate to predict hydrate decomposition and soil deformation.

3. NUMERICAL SIMULATIONS

3.1. Numerical Method. Hydrate decomposition mainly includes four processes: phase change, heat conduction, seepage process, and stress propagation. The characteristic time tables of these four processes are described as phase transition, heat conduction, percolation process, and stress propagation, respectively. Moreover, the dimensionless representation of the four processes are $\frac{\rho_h}{k_d \cdot (p_e - p_g) \cdot A_s}$, $\frac{h^2}{k_s}$, $\frac{h}{\sqrt{\frac{E_s}{r_s}}}$, and $\frac{\mu \cdot h^2}{k \cdot (p_g - p_d)}$, respectively,[42] where k_s is the thermal conductivity of the soil skeleton (3 W/(m·K)), μ is the gas viscosity coefficient (10^{-5} Pa·s), k is the permeability of the sedimentary layer (10^{-16} m^2), E_s is the elastic modulus of the sediment (5×10^8 Pa), k_d is the kinetic constant of hydrate phase transition (4.4×10^{-16} kg/(s·Pa·m^2)), ρ_h is the hydrate density (910 kg/m^3), h is the hydrate sediment area (1 m), p_d is the constant pressure at the reduced pressure (2.5×10^6 Pa), p_e is the pressure when the hydrate phase is in equilibrium, and p_g is the gas pressure.

The ratio between these four quantities and their results is[42]

$$t_c : t_d : t_p : t_s = 10^9 : 10^7 : 10^6 : 1 \tag{17}$$

Therefore, it is clear that the stress propagation is the fastest, the heat conduction process is the slowest, and the magnitude of the four numbers differs greatly; hence, decoupling analysis can be performed.

According to the ratio of the characteristic time of these four physical processes, the stress wave propagates the fastest, while the heat conduction process is the slowest. The seepage process is 3 orders of magnitude faster than the heat conduction process, and the stress propagation is 6 orders of magnitude faster than the seepage process. Therefore, the hydrate decomposition process can be decoupled analysis. In the later analysis of this work, we can temporarily ignore the hydrate decomposition process and only consider the impact of hydrate decomposition on the mechanical deformation of the overlying soil.

The following simulation is mainly for analyzing soil deformation caused by hydrate decomposition. First, the initial conditions, including the pore pressure, reservoir temperature, boundary-given pressure, and initial hydrate saturation, along with the constants, including the seepage coefficient, molar fraction of methane gas, hydrate pore pressure, and hydrate density at equilibrium, are assigned. Subsequently, the internal pressure of the hydrate zone is changed in accordance with time and position. The change in the saturation of the hydrate with time and position under a specific pressure drop is obtained. The fracture stress of the hydrate deposit layer can be calculated based on the change in hydrate saturation,[43,44] which, over time and position, can be calculated using eq 17 proposed by Zhou et al.[41] The calculation parameters are set according to the sediment parameters of the offshore water.

In the actual hydrate exploration, the hydrate saturation changes with both location and time. The function of the damage strength with location and time is proposed below.

The hydrate decomposition rate can be obtained using the following formula[45]

$$\frac{\partial S_h}{\partial t} = \frac{K_d M_g A_s (p_e - p)}{\rho_h} \tag{18}$$

https://dx.doi.org/10.1021/acsomega.0c05463
ACS Omega 2021, 6, 5335−5347

where K_d is the coefficient, M_g is the mole fraction of methane gas, A_s is the surface area, p_e is the pore pressure at hydrate equilibrium, and p is the real-time pore pressure.

According to the above formula, when p changes with time, the change in S_h with time can be solved. Equation 18 can then be used to obtain the stress−strain relationship and the change in failure stress over time. Taking p as a constant and an example and ignoring the change in surface area, the following expression can be obtained.

$$S_h = S_{ho} - \frac{K_d M_g A_g (p_e - p)t}{r} \tag{19}$$

where S_{ho} is the initial hydrate saturation.

Considering decompression mining as an example, if the given pressure at the boundary is p_0, the internal pressure is p_1, and the spatial scale is 1, then the change in pore pressure with time and space position is as follows

$$p = p_1 + \frac{p_0 - p_1}{l}x + \sum_{n=0}^{\infty} \frac{2(p_0 - p_1)}{n\pi} e^{-(n^2\pi^2 a^2/l^2)t} \sin\frac{n\pi}{l}x$$

$$a^2 = \frac{K}{\mu \cdot \phi \cdot c_t} \tag{20}$$

The destructive stress relationship is expressed as below.

$$\varepsilon_d < 25\%,\ \tau_s = 0.267 + 4.34(S_{ho} - K_d M_g A_s (p_e - p)t)$$

$$\varepsilon_d \geqslant 25\%,\ \tau_s = 2.14 - 2.9(S_{ho} - K_d M_g A_s (p_e - p)t) + 6.5(S_{ho} - K_d M_g A_s (p_e - p)t)^2 \tag{21}$$

Equation 21 reflects the variations in the failure stress with the production time of hydrate. Therefore, the destructive pressure can be expressed as a function of both location and time.

3.2. Analysis of Calculation Results. This study focuses on changes in the decomposition range with decomposition time. It is assumed that the one-dimensional hydrate deposit layer is 200 m long. The trial exploitation of hydrates in the South China Sea during 2017 was conducted for 60 days. Therefore, the test exploitation durations were set to 3, 7, 14, 21, 28, 40, and 60 days, and the tested degrees of pressure reduction were 3, 6, and 9 MPa, respectively. The hydrate decomposition range was analyzed at different times and pressures under these 21 conditions (days and depressurization). When using MATLAB for unit division, the length is in meters and the time is in hours.

The change in the hydrate decomposition range over time with a pressure drop of 3 MPa is shown in Figure 5. When the depressurization duration is below 1 week, the decomposition range does not change greatly. As the depressurization duration increases, the decomposition range gradually increases. As the pressure is decreased only by 3 MPa, the hydrate decomposition rate is relatively slow, resulting in a slower decrease in hydrate saturation in the sedimentary layer. Therefore, the rate of change in the decomposition range is low.

The effect of the degree of depressurization on the decomposition range is shown in Figure 6. When the depressurization duration is constant and the degree of decompression is large, the hydrate decomposition rate is accelerated, reducing the hydrate content in the sedimentary layer and resulting in soil deformation and a larger decomposition range. Figure 7 presents the decomposition range over time at different degrees of depressurization. When

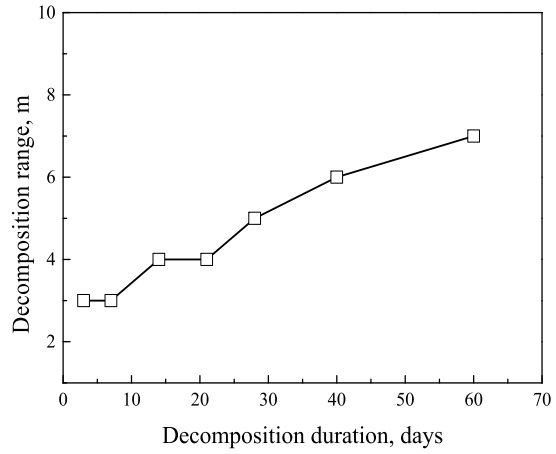

Figure 5. Decomposition range with decomposition time with 3 MPa of depressurization.

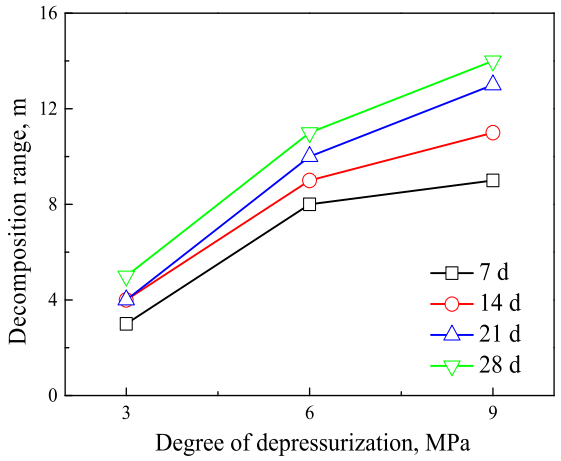

Figure 6. Decomposition range under different degrees of depressurization at the same duration.

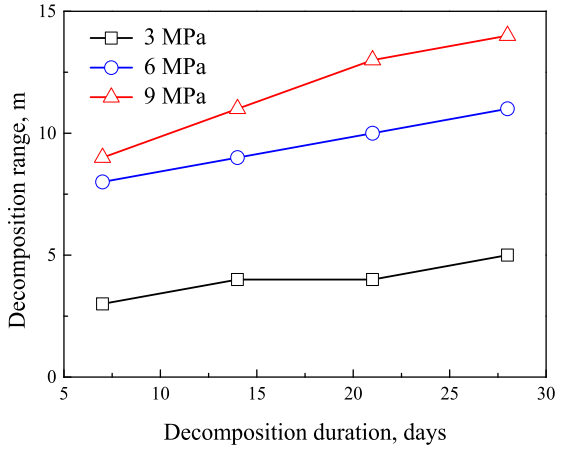

Figure 7. Decomposition range at different durations under the same degree of depressurization.

https://dx.doi.org/10.1021/acsomega.0c05463
ACS Omega 2021, 6, 5335−5347

the decompression pressure is increased to 6 and 9 MPa, the rate of change in the decomposition range over time is significantly higher. The change in the decomposition range is the highest when the degree of pressure reduction is 9 MPa.

Under a pressure decrease of 3 MPa and depressurization durations of 3, 7, 14, and 21 days, the hydrate decomposition range is relatively stable. In the previous unit division, the length interval was 1 m, which may have caused the small change in the decomposition range. To verify this, the length interval was reduced to 0.1 m to investigate the differences in the decomposition range at depressurization durations of 3, 7, 14, and 21 days. The decomposition range at different depressurization durations with a length interval of 0.1 m and a pressure drop of 3 MPa is shown in Table 2.

Table 2. Decomposition Range for a Pressure Drop of 3 MPa

depressurization duration (day)	decomposition range (m)
3	3.4
7	3.8
14	4.3
21	4.8

As shown in Table 2, the decomposition range varies slowly over time, and the effect of this change on sediment deformation is negligible.

Utilizing the theoretical analysis and MATLAB calculation, the hydrate saturation at different times and locations is obtained, and the failure stress of each soil layer is obtained using eq 21.

4. SENSITIVITY ANALYSIS OF TRIAL EXPLOITATION IN OFFSHORE WATERS

During the trial exploitation of hydrate, the decomposition range is limited. In addition to research work, such as logging conducted before and after the trial exploitation, it is necessary to evaluate the local hydration around the wellbore, stability of the sediment layer, and overlying layer, considering that the impact range is within a few meters or tens of meters. This study mainly focuses on the factors that may affect the stability of the local hydrate soil and the overlying layers around the wellbore during the hydrate exploitation process. The specific hydrate decomposition phase transformation process is not considered here; only the changes in stress distribution and numerical displacement in the case of step-down decomposition are studied.

4.1. Numerical Model of Trial Exploitation. Taking the geological features of the offshore waters of China as a reference, as shown in Figure 8, the sediment layer is divided into three parts: the overlying layer, hydrate layer, and lower soil layer, with thicknesses of 140, 10−30, and 100−200 m, respectively. The seawater depth in the calculation model is 1000 m, and the sediment thickness is 275 m. To eliminate the boundary effect, both the length and width are set to 800 m, which is more than twice the sediment thickness. The wellbore passed through the lower soil layer. The outer diameter of the cylinder wall is 0.024 m, and the wall thickness is 0.002 m. Before the decomposition of the hydrate layer, the modulus is 100 MPa, and the density is 1700 kg/m^3. When using the model to simulate the situation in the trial exploitation area, the soil parameters in this area are obtained from on-site exploration using real data. Following decomposition, the

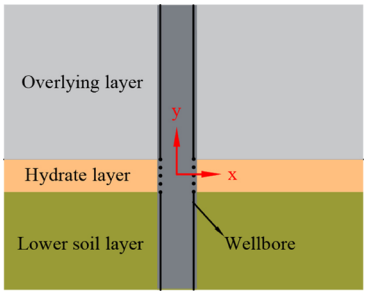

Figure 8. Schematic of the wellbore and sediment layers.

modulus changes to 37 MPa, while density remains constant. The modulus of the overlying layer is 3−20 MPa, which increases linearly with depth. Additionally, the density increases linearly from 1360 to 1700 kg/m^3 with depth. The lower soil layer has a modulus of 30 MPa and a density of 4500 kg/m^3. The wellbore modulus and density are 0.152 MPa and 7890 kg/m^3, respectively.

Initially, the ground stress balance is calculated to eliminate the vertical displacement caused by the weight of the wellbore and soil, and the deformation of the overlying layer caused by hydrate decomposition and sediment deformation in the hydrate zone are analyzed. Assuming that the hydrate is decomposed, there is no change in pore pressure due to the high permeability of the formation. Therefore, the calculation model is considered based on the elastoplastic theory and analyzed using the Mohr−Coulomb constitutive model. The upper surface of the model is a free surface, the left and right boundaries are fixed in the x-direction, and the bottom edge is fixed in the y-direction. The model is divided into 490,944 units, and the wellbore is simulated as the pile unit. Two scenarios are considered in the calculation: (1) the strength of the formation is greatly reduced after hydrate decomposition, and the sediment is washed away and collapses to form a cavity goaf without any load; (2) after decomposition, the sediment softens and can withstand part of the load. In the numerical simulation, the cavity goaf is realized by setting the null model.

The calculation is conducted under the following conditions for comparative analysis:

(1) The hydrate decomposition zone is a cylinder with a radius and height of 3.5 and 10 m, respectively, and the dip angles of the submarine sediment layer are 3°, 9°, and 15°.
(2) The dip angle of the seabed soil layer is 3°, and four hydrate decomposition zones with different sizes are considered, as follows: a radius and height of 3.5 and 10 m, a radius and height of 12.5 and 20 m, a radius and height of 18.5 and 26 m, and a radius and height of 24.5 and 30 m.
(3) The hydrate decomposition zone is a cylinder with a radius of 3.5 m and a height of 10 m, and the sediment softens after decomposition.

The sediment deformation around the wellbore and the effect of slope angle and decomposition range on deformation are analyzed by calculation.

4.2. Effect of Dip Angle. Figure 9 shows the vertical displacement of hydrate under the goaf condition. The 0 point of the x-axis represents the position of the wellbore. During hydrate decomposition with a zone radius and height of 3.5 and 10 m, respectively, the vertical displacement of the upper surface of the goaf is significantly smaller at an inclination angle

https://dx.doi.org/10.1021/acsomega.0c05463
ACS Omega 2021, 6, 5335−5347

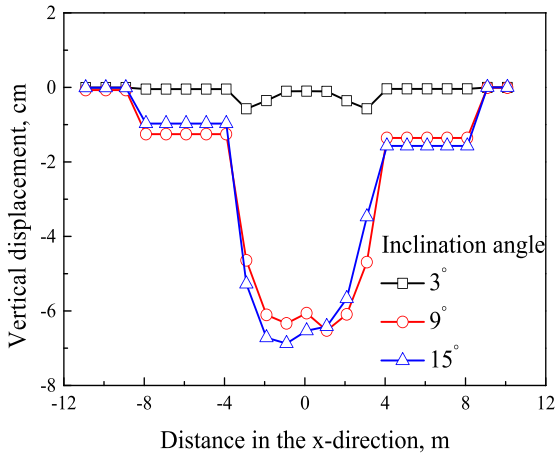

Figure 9. Vertical displacement of hydrate under the goaf condition.

of 3° than that at inclination angles of 9° and 15°. At a dip angle of 3°, the maximum vertical displacement is 0.8 cm. As the inclination angle increases from 3° to 9°, the vertical displacement increases by approximately 12 times. Although the maximum vertical displacement at a dip angle of 3° is 6.7 cm, the overall vertical displacement is still small in comparison to the decomposition range, which will not cause sediment collapse because of the vertical displacement experienced by the soil under gravity, when the hydrate decomposition area is mined. The larger the inclination angle, the larger the displacement. However, owing to the small decomposition range, the displacement is relatively small under the influence of the soil modulus and internal friction angle, which will not cause soil damage.

Figure 10 shows the horizontal displacement of hydrate under the goaf condition. At an inclination angle of 3°, the soil

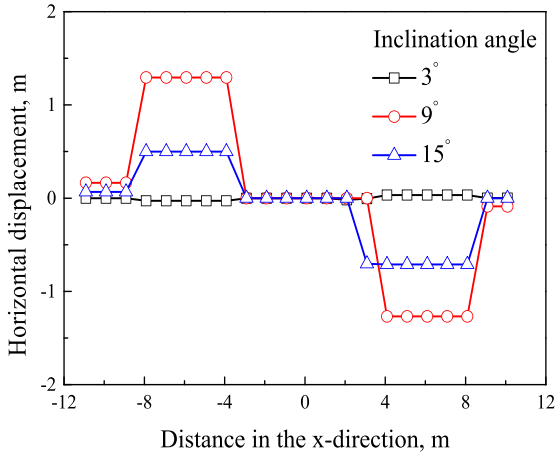

Figure 10. Horizontal displacement of hydrate under the goaf condition.

surrounding the goaf outwardly expands in the horizontal direction, possibly because of the small decomposition zone and the outward expansion of sediment around the goaf due to vertical displacement. At dip angles of 9° and 15°, the soil around the goaf is compressed. Therefore, the horizontal displacement is small compared to the decomposition range, and no sediment damage occurs. Owing to the small hydrate decomposition range, the overall deformation of the soil layer is small within the range of inclinations considered in the calculation.

4.3. Impact of Changes in the Size of the Decomposition Zone. In all four cases, the maximum vertical displacement occurs on both sides of the wellbore near the edge of the goaf (Figure 11). As the size of the

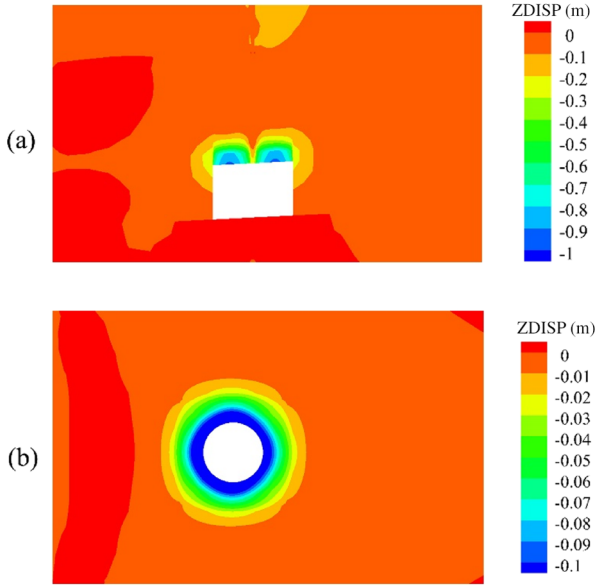

Figure 11. Cloud map of vertical subsidence: (a) side view and (b) top view.

decomposition zone gradually increases, the maximum vertical displacement of the soil correspondingly increases (Figure 12).

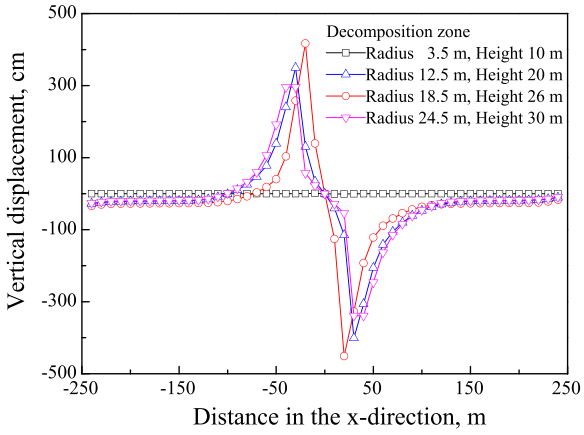

Figure 12. Overburden settlement under the goaf condition in the hydrate decomposition zone.

To evaluate the impact of the hydrate decomposition range on the soil displacement, this paper simulates four situations. As can be seen from Figure 12, when the decomposition range of hydrate gradually expands, the displacement of the soil also increases continuously. When the decomposition radius reaches 24.5 cm, the soil collapses and the calculation process is aborted. Both the modulus and cohesive force are small, causing shear failure to occur in the overlying soil, which creates a nonconvergence condition in the numerical simulation. When the height of the goaf is 3.5 or 12.5 m, the soil above the goaf does not undergo significant vertical

https://dx.doi.org/10.1021/acsomega.0c05463
ACS Omega 2021, 6, 5335−5347

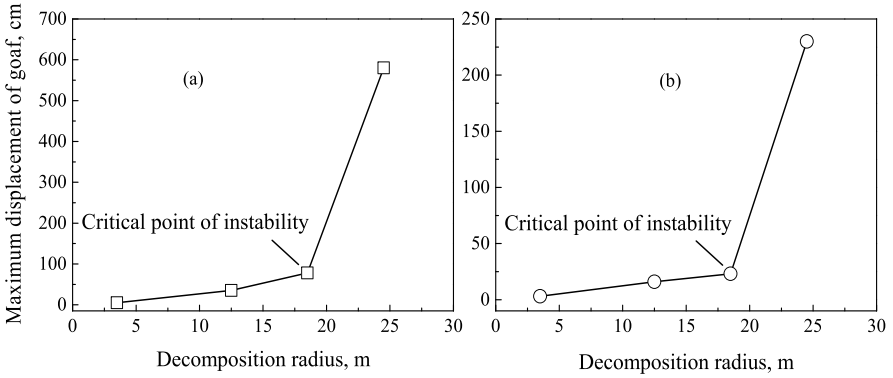

Figure 13. Displacement of goaf in the hydrate decomposition zone: (a) vertical and (b) horizontal.

displacement. Further, when the goaf size reaches 18.5 × 26 m, the vertical strain reaches 6%. However, when the size exceeds 18.5 × 26 m, soil deformation increases sharply, and the sediment layer quickly deforms and is destroyed. This value can be taken as the critical point of deformation and failure of the wellhead soil layer under the goaf condition. Therefore, in practice, the decomposition range should be controlled within this critical value (Figure 13). Vertical displacement mainly occurs in the upper part of the goaf (Figure 13a), whereas horizontal displacement tends to be restricted around the goaf (Figure 13b). This simulation is mainly used to investigate that during the exploitation process, the decomposition range of hydrates will gradually become larger, which may eventually cause the overlying soil to collapse and interrupt the exploitation process. When the thickness of the overburden soil, the inclination of the hydrate reservoir, the hydrate exploitation time, or the mechanical properties of the overburden soil change, resimulation is necessary for the evaluation.

It will vary with geological characteristics. For different geological conditions, it is necessary to perform numerical simulation again to find the critical point.

4.4. Comparison of Goaf and Softening in the Decomposition Zone. The variation in the vertical displacement with changes in the inclination angle of the seabed sediment layer at a decomposition radius of 3.5 m and a height of 10 m is presented in Figure 14. At an inclination angle of 3°, the vertical displacement is small. The vertical displacement increases significantly at an inclination angle of 9° under the action of gravity. Moreover, at an inclination angle of 15°, large-area plastic failure in the soil causes the calculation to terminate, resulting in a smaller calculated vertical displacement than that at an inclination angle of 9°. The calculation result is not accurate; thus, the vertical displacement at an inclination angle of 15° is not plotted in this figure. However, generally, the magnitude of vertical displacement is small. At an inclination angle of 3°, the vertical displacement is 0.7 cm. When the soil layer in the hydrate decomposition zone softens, the increase in the slope does not significantly affect the vertical displacement of the soil.

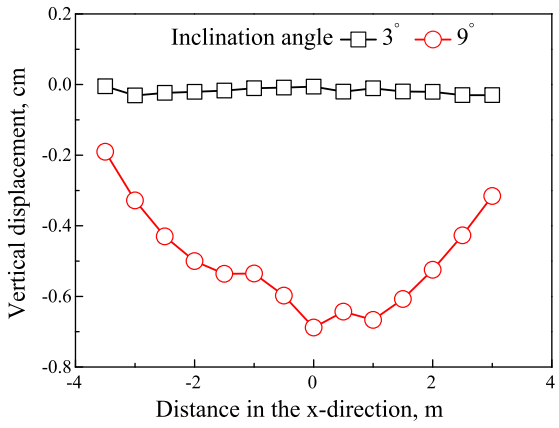

Figure 14. Settlement of the hydrate decomposition zone under sediment layer softening.

As shown in Figure 15, when the sediment in the decomposition zone is softened, the soil on both sides of the exploitation shaft moves to the middle. The horizontal displacement on both sides of the exploitation shaft for the inclination angle of 9° is larger than that for an inclination angle of 3°. The reason for this phenomenon is that the force that pushes the soil to the middle is larger for the inclination angle of 9°. However, the compressional deformations are small in magnitude for the two inclination angles, and the maximum horizontal displacement is less than 1.3 cm.

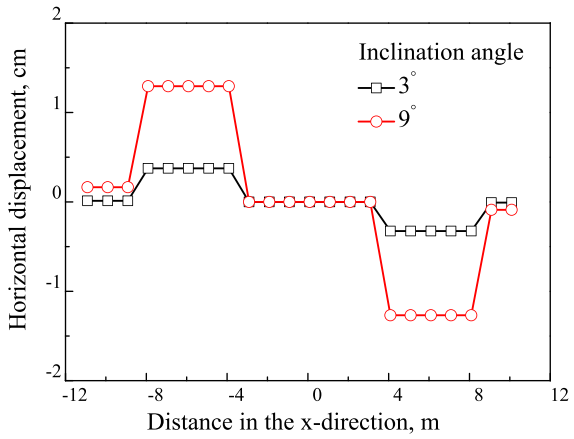

Figure 15. Horizontal displacement of the hydrate decomposition zone under sediment layer softening.

With the increase in the decomposition range, the deformation of the soil layer increases continuously. The vertical settlement reaches 3.5 cm when the radius of the decomposition zone is 24 m (Figure 16a). The horizontal displacement is mainly represented by the extrusion wellbore. When the radius of the decomposition zone is 24 m, the maximum horizontal displacement reaches 4.5 cm, with the

https://dx.doi.org/10.1021/acsomega.0c05463
ACS Omega 2021, 6, 5335−5347

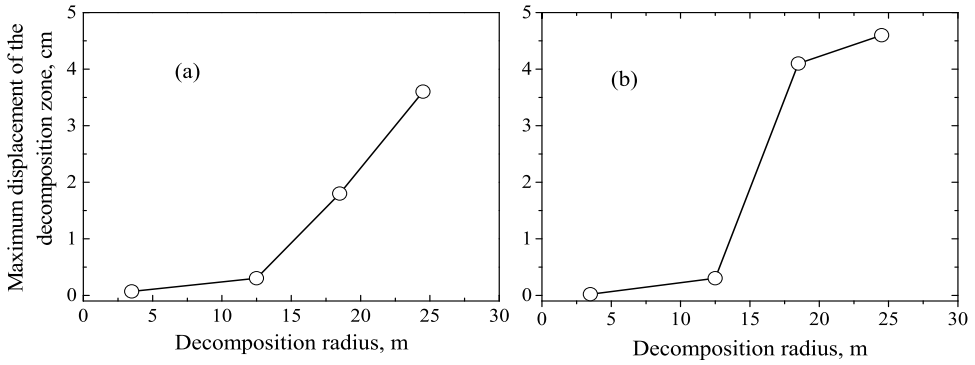

Figure 16. Displacement of the decomposition zone under soil softening in the hydrate decomposition zone: (a) vertical and (b) horizontal.

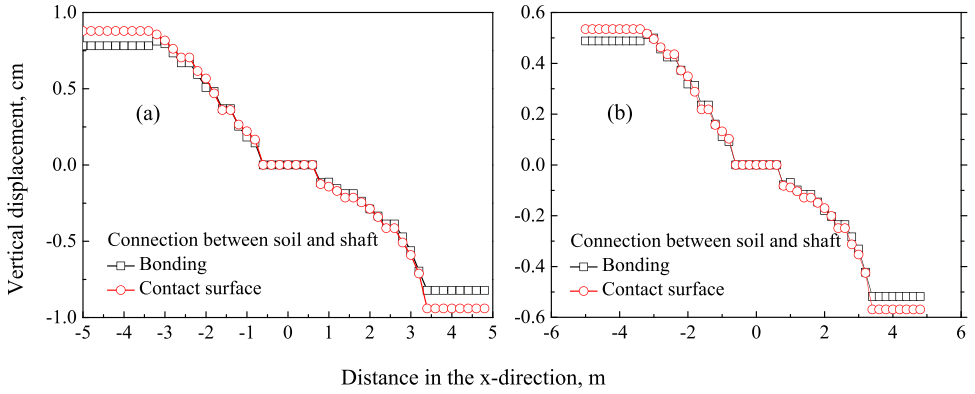

Figure 17. Comparison of the local settlement of the overlying soil: (a) exploiting and (b) softening.

damaged state temporarily distant (Figure 16b). However, according to Figures 13 and 16, in the trial exploitation process, the decomposition range gradually increases with the trial exploitation duration, increasing the possibility of soil destruction.

With the increasing demand for energy, the technology of exploiting and using hydrates is urgently needed to survive the crisis of energy depletion. This paper analyzes the local geological disasters caused by the decomposition of hydrates and the inclination of the soil and the decomposition range. These results can be used to evaluate the safety of hydrate exploitation and avoid collapse accidents during exploitation. In the process of hydrate decomposition, there are a complete decomposition zone and incomplete decomposition zone. However, the area of incomplete decomposition is very small and has little influence on the stability analysis of the soil. Therefore, the future safety assessment of the on-site exploitation situation can only consider the complete decomposition of hydrate.

4.5. Effect of Connection States between Soil and Shaft. The horizontal displacement and maximum stress of the wellbore in the formation increase with the increase in the hydrate decomposition range. As the hydrate decomposition range expands with an overlying layer, the wellbore gradually develops from elastic deformation to overall dumping.[46] However, in this work, considering the stability of the soil during the exploitation process in the hydrate area, the decomposition range will not reach the level of causing serious bending of the steel pipe. Therefore, this section only considers the influence of the connection between the shaft and the soil on the settlement of the soil.

When the inclination angle of the submarine soil layer is 3°, the decomposition zone is 3.5 m in radius and 10 m in height; the local settlement of the overlying soil for two connection states is shown in Figure 17. Regardless of whether the hydrate decomposition zone is in the limit state of excavation or the state of soil softening, the deformation of the soil when the soil is in contact with the shaft (allowing vertical relative sliding) is greater than that when the soil is bonded to the shaft. It can be seen that when the soil and the wellbore are in a bonded state, the interaction between the soil and the wellbore affects the settlement of the wellbore and the surrounding soil, making a slightly larger settlement of the wellbore and a smaller settlement of the surrounding soil.

When the inclination angle of the submarine soil layer is 3°, the decomposition zone is 3.5 m in radius and 10 m in height; the local settlement on the top surface of goaf for two connection states is shown in Figure 18. When there is a contact surface between the shaft and the soil, the settlement of the soil is relatively larger, while the settlement of the shaft is relatively smaller. This is due to the fact that when there is a contact surface between the shaft and the soil, there is slippage between the shaft and the soil. Therefore, the mutual influence between the shaft and the soil is small. When the soil is bonded to the shaft, the settlement of the shaft becomes larger due to the interaction, and the settlement of the surrounding soil is relatively small.

When the inclination angle of the submarine soil layer is 3°, the decomposition zone is 3.5 m in radius and 10 m in height; the local settlement of the soil in the decomposition zone without passing through the shaft for two connection states is shown in Figure 19. In the two cases, the trend of soil settlement is the same. When there is a contact surface

https://dx.doi.org/10.1021/acsomega.0c05463
ACS Omega 2021, 6, 5335−5347

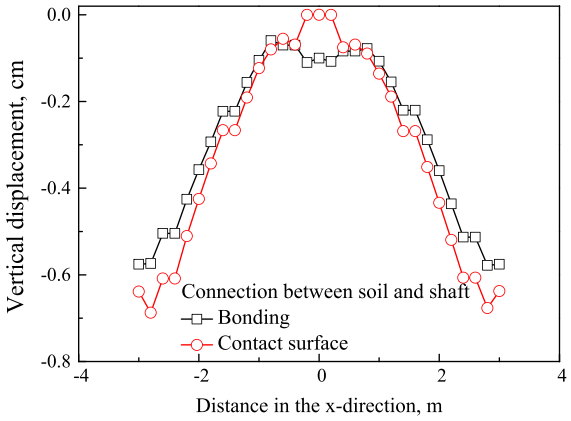

Figure 18. Comparison of the local settlement on the top surface of goaf.

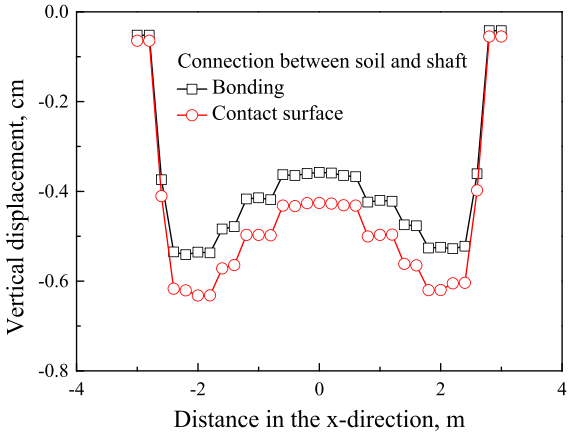

Figure 19. Comparison of the local settlement on the top surface of goaf that does not pass through the shaft.

between the shaft and the soil, the settlement of the soil is relatively larger. In the limit of the exploited out soil in the decomposition area, the maximum displacement of the soil settlement occurs at the edge of the exploited out area.

As discussed above, the connection between the shaft and the soil has an impact on the settlement of the soil. When the wellbore and the soil are bonded to each other, due to the interaction, the settlement of the wellbore is slightly larger, and the settlement of the soil around the wellbore is slightly smaller. When the soil and the shaft are connected by a contact surface, the interaction force is reduced, and there is slippage between the soil and the shaft. Therefore, the settlement of the soil around the shaft is larger, and the settlement of the pile is reduced.

5. CONCLUSIONS

The decomposition range of hydrates in a certain time under reduced pressure conditions includes incomplete and complete decomposition regions. However, during the exploitation process, the area where the hydrate is not completely decomposed is small, which basically does not affect the safety assessment of the settlement of the soil around the wellhead due to the decomposition of the hydrate. Therefore, the safety assessment of the exploitation area mainly focuses on the complete decomposition of the hydrate area.

When the dip angle of the seabed sediment layer is constant, the decomposition area and soil deformation increase continuously. When the decomposition range is below a certain critical value, the deformation is limited and no collapse occurs. However, once this critical value is exceeded, the sediment around the decomposition zone is shear-damaged. Therefore, the exploitation process must pay attention to below the critical value.

Under offshore field conditions, within 1 week of decompression and exploitation, the hydrate decomposition radius is approximately 3 m. With increases in the inclination of the seabed soil layer, the soil deformation in the decomposition zone gradually increases under the effect of gravity. For example, as the inclination angle increases from 3° to 9°, the sediment deformation increases by 12 times; however, the overall settlement is low. The settlement at an inclination angle of 9° is only 6.7 cm, which would not cause sediment collapse.

Via the analysis of three sensitive parameters, including the soil dip angle, the decomposition range, and the connection states between the soil and the shaft, it can be seen that the soil dip angle has little effect on the settlement of hydrate soil and will not cause a large area of soil collapse during the exploitation process. In the process of hydrate exploitation, with a gradual decomposition of hydrate caused by pressure reduction, the decomposition area of the hydrate sediment layer gradually increases, the soil-bearing capacity gradually increases, and the soil-bearing capacity gradually decreases. This will lead to a local collapse of the exploitation site due to the shear deformation after a certain period of exploitation.

When the mechanical properties of the soil and the geological structure are different, the critical values of the soil collapse caused by the expansion of the hydrate decomposition area are different. To ensure the accuracy of the safety assessment of the hydrate exploitation, the numerical simulation needs to be repeated for different exploitation points. In the actual exploitation process, the critical value must be estimated in advance according to the mechanical properties of the on-site soil to ensure safety.

AUTHOR INFORMATION

Corresponding Author

Guangrui Sun − *Department of Mechanical Engineering, National University of Singapore, 117576, Singapore;* orcid.org/0000-0003-1432-616X; Email: mpesung@nus.edu.sg

Authors

Lele Yang − *School of Civil Engineering and Transportation, South China University of Technology, Guangzhou 510641, China; School of Marine Engineering and Technology, Sun Yat-sen University, Guangzhou 510275, China;* orcid.org/0000-0002-8621-8697

Jing Wang − *School of Marine Engineering and Technology, Sun Yat-sen University, Guangzhou 510275, China*

Yongliang Yang − *Department of Mechanical Engineering, National University of Singapore, 117576, Singapore*

Complete contact information is available at: https://pubs.acs.org/10.1021/acsomega.0c05463

Notes

The authors declare no competing financial interest.

https://dx.doi.org/10.1021/acsomega.0c05463
ACS Omega 2021, 6, 5335−5347

■ ACKNOWLEDGMENTS

This work was financially supported by the Basic and Applied Basic Research Fund of Guangdong Province of China (no. 2020A1515110155), the China Postdoctoral Science Foundation (nos. 2019M663242 and 2020T130749), and the Fundamental Research Funds for the Central Universities (no. 19lgpy86).

■ REFERENCES

(1) Koh, C. A. Towards a fundamental understanding of natural gas hydrates. *Chem. Soc. Rev.* **2002**, *31*, 157−167.
(2) Sloan, E. *Clathrate hydrates of natural gases*. Marcel Dekker, Inc.: New York, 1998.
(3) Wilder, J. W.; Seshadri, K.; Smith, D. H. Modeling hydrate formation in media with broad pore size distributions. *Langmuir* **2001**, *17*, 6729−6735.
(4) Henry, P.; Thomas, M.; Clennell, M. B. Formation of natural gas hydrates in marine sediments: 2. Thermodynamic calculations of stability conditions in porous sediments. *J. Geophys. Res.: Solid Earth* **1999**, *104*, 23005−23022.
(5) Clauser, S.; Renard, M.; Richebois, G. *Proceedings of the Ocean Drilling Program*; Ocean Drilling Program, Texas A&M University: 1988.
(6) Kvenvolden, K. A.; Lorenson, T. D. Global occurrences of gas hydrate. In *The Eleventh International Offshore and Polar Engineering Conference*; International Society of Offshore and Polar Engineers:, 2001.
(7) Kondori, J.; Zendehboudi, S.; Hossain, M. E. A review on simulation of methane production from gas hydrate reservoirs: Molecular dynamics prospective. *J. Pet. Sci. Eng.* **2017**, 1−772.
(8) Kvenvolden, K. A.; Lorenson, T. D. The global occurrence of natural gas hydrate. In *Natural Gas Hydrates: Occurrence, Distribution, and Detection: Occurrence, Distribution, and Detection*; American Geophysical Union: 2001, *124*, 3−18, DOI: 10.1029/GM124p0003.
(9) Milkov, A. V. Global estimates of hydrate-bound gas in marine sediments: how much is really out there? *Earth-Sci. Rev.* **2004**, *66*, 183−197.
(10) Klauda, J. B.; Sandler, S. I. Global distribution of methane hydrate in ocean sediment. *Energy Fuels* **2005**, *19*, 459−470.
(11) Ruppel, C. Tapping methane hydrates for unconventional natural gas. *Elements* **2007**, *3*, 193−199.
(12) Collett, T. S. S.; Boswell, R.; Lee, M. W. W.; Anderson, B. J. J.; Rose, K.; Lewis, K. A. A. Evaluation of long-term gas-hydrate-production testing locations on the Alaska North Slope. *SPE Reservoir Eval. Eng.* **2012**, *15*, 243−264.
(13) Collett, T. S. Gas hydrate reservoir properties. In *Unconventional Resources Technology Conference*; Society of Exploration Geophysicists, American Association of Petroleum: 2013; pp 1929−1937.
(14) Collett, T. S. Reservoir controls on the occurrence and production of gas hydrates in nature. In *Offshore Technology Conference*; Offshore Technology Conference: 2014.
(15) Kimoto, S.; Oka, F.; Fushita, T.; Fujiwaki, M. A chemo-thermo-mechanically coupled numerical simulation of the subsurface ground deformations due to methane hydrate dissociation. *Comput. Geotech.* **2007**, *34*, 216−228.
(16) Stevens, J. C.; Howard, J. J.; Baldwin, B. A.; Ersland, G.; Husebø, J.; Graue, A. Experimental hydrate formation and gas production scenarios based on CO2 sequestration. In *Proceedings of the 6th International Conference on Gas Hydrates*; The University of British Columbia: 2008; pp. 6−10.
(17) Fangzhen, J.; Jianhui, F.; Jizheng, Y.; Xunyu, C.; Faqi, H. Direction, key factors and solution of marine natural gas exploration in Yangtze area. *China Pet. Explor.* **2015**, *20*, 1−8.
(18) Terao, Y.; Lay, K.; Yamamoto, K. Design of the surface flow test system for 1st offshore production test of methane hydrate. In *Offshore Technology Conference-Asia*; Offshore Technology Conference: 2014.
(19) Fujii, T.; Noguchi, S.; Takayama, T.; Suzuki, K.; Yamamoto, K.; Saeki, T. Site selection and formation evaluation at the 1st offshore methane hydrate production test site in the eastern Nankai Trough, Japan. In *75th EAGE Conference & Exhibition-Workshops*; European Association of Geoscientists & Engineers: 2013; pp cp-349-00010.
(20) Wenke, F.; Yaohong, S.; Linghui, C. Research for seafloor landslide stability on the outer continental shelf and the upper continental slope in the northern South China Sea. *Mar. Geol. Quat. Geol.* **1994**, *14*, 81−94.
(21) Wu, B.-X.; Lei, H.-Y. Experimental simulation on equilibrium temperature and pressure of methane hydrate in sediment systems. *Pet. Explor. Dev.* **2004**, *31*, 22−24.
(22) Bouriak, S.; Vanneste, M.; Saoutkine, A. Inferred gas hydrates and clay diapirs near the Storegga Slide on the southern edge of the Vøring Plateau, offshore Norway. *Mar. Geol.* **2000**, *163*, 125−148.
(23) Winters, W. J.; Waite, W. F.; Mason, D. H.; Gilbert, L. Y.; Pecher, I. A. Methane gas hydrate effect on sediment acoustic and strength properties. *J. Pet. Sci. Eng.* **2007**, *56*, 127−135.
(24) Zhang, X.-h.; Shu-yun, W.; Qing-ping, L. Experimental study of mechanical properties of gas hydrate deposits. *Rock Soil Mech.* **2010**, *31*, 3069−3074.
(25) Zhang, H.; Zhu, Y. Survey and research on gas hydrate in permafrost region of China. *Geol. Bull. China* **2011**, *30*, 1809−1815.
(26) Yamamoto, K. Methane hydrate bearing sediments: a new subject of geomechanics. In *The 12th International Conference of International Association for Computer Methods and Advances in Geomechanics (IACMAG)*; IACMAG: 2008; pp. 1−6.
(27) Carpenter, G. Coincident sediment slump/clathrate complexes on the U.S. Atlantic continental slope. *Geo-Mar. Lett.* **1981**, *1*, 29−32.
(28) Shi, Y. H.; Zhang, X. H.; Lu, X. B.; Wang, S. Y.; Wang, A. L. Experimental Study on the Static Mechanical Properties of Hydrate-Bearing Silty-Clay in the South China Sea. *Chin. J. Theor. Appl. Mech.* **2015**, *47*, 521−528.
(29) Yoneda, J.; Takiguchi, A.; Ishibashi, T.; Yasui, A.; Mori, J.; Kakumoto, M.; Aoki, K.; Tenma, N. Mechanical Response of Reservoir and Well Completion of the First Offshore Methane-Hydrate Production Test at the Eastern Nankai Trough: A Coupled Thermo-Hydromechanical Analysis. *Soc. Pet. Eng. J.* **2018**, 1−546.
(30) Nixon, M. F.; Grozic, J. L. H. Submarine slope failure due to gas hydrate dissociation: a preliminary quantification. *Can. Geotech. J.* **2007**, *44*, 314−325.
(31) Acosta, E. A.; Tibana, S.; de Almeida, M. D. S. S.; Saboya, F., Jr. Centrifuge modeling of hydroplaning in submarine slopes. *Ocean Eng.* **2017**, *129*, 451.
(32) Zhang, X. H.; Lu, X. B.; Chen, X. D.; Zhang, L. M.; Shi, Y. H. Mechanism of soil stratum instability induced by hydrate dissociation. *Ocean Eng.* **2016**, *122*, 74−83.
(33) Yousif, M. H.; Abass, H. H.; Selim, M. S.; Sloan, E. D. Experimental and theoretical investigation of methane-gas-hydrate dissociation in porous media. *SPE Reservoir Eng.* **1991**, *6*, 69−76.
(34) Ng, A.; Klar, A.; Soga, K. Coupled Soil Deformation-Flow-Thermal Analysis of Methane Production in Layered Methane Hydrate Soils. In *Offshore Technology Conference*; Offshore Technology Conference: 2008.
(35) Lee, S.-R.; Kim, S.-J. Onshore and offshore gas hydrate production tests. *Econ. Environ. Geol.* **2014**, *47*, 275−289.
(36) Yamamoto, K.; Terao, Y.; Fujii, T.; Ikawa, T.; Seki, M.; Matsuzawa, M.; Kanno, T. Operational overview of the first offshore production test of methane hydrates in the Eastern Nankai Trough. In *Offshore Technology Conference*; Offshore Technology Conference: 2014.
(37) White, M. D.; Kneafsey, T. J.; Seol, Y.; Waite, W. F.; Uchida, S.; Lin, J. S.; Myshakin, E. M.; Gai, X.; Gupta, S.; Reagan, M. T.; Queiruga, A. F.; Kimoto, S. An international code comparison study on coupled thermal, hydrologic and geomechanical processes of natural gas hydrate-bearing sediments. *Mar. Pet. Geol.* **2020**, 104566.
(38) Pearson, C. F.; Halleck, P. M.; McGuire, P. L.; Hermes, R.; Mathews, M. Natural gas hydrate deposits: a review of in situ properties. *J. Phys. Chem.* **1983**, *87*, 4180−4185.

https://dx.doi.org/10.1021/acsomega.0c05463
ACS Omega 2021, 6, 5335−5347

(39) Lui, B.; Han, Y. *FLAC principle examples and application guide*; China Communications Press: 2005.
(40) Zendehboudi, S.; Rezaei, N.; Lohi, A. Applications of hybrid models in chemical, petroleum, and energy systems: A systematic review. *Appl. Energy* **2018**, *228*, 2539−2566.
(41) Zhou, M.; Soga, K.; Xu, E.; Uchida, S.; Yamamoto, K. Numerical study on Eastern Nankai Trough gas hydrate production test. In *Offshore Technology Conference*; Offshore Technology Conference: 2014.
(42) Zhang, X.-H. Study on softening and destruction of hydrate deposits due to thermal decomposition of hydrate. Ph.D. thesis; University of Chinese Academy of Science, 2010.
(43) Hong, H.; Pooladi-Darvish, M.; Bishnoi, P. R. Analytical modelling of gas production from hydrates in porous media. *J. Can. Pet. Technol.* **2003**, *42*, 45−56.
(44) Liu, L. Evolution of gas hydrate dissociation front in hydrate bearing sediment. Ph.D. thesis; Institute of Mechanics, Chinese Academy of Sciences, China, 2013.
(45) Lu, X.-B.; Zhang, X.-H.; Shi, Y.-H.; et al. Mechanical properties of hydrate-bearing silty-clay and stress-strain relation. *Period. Ocean Univ. China* **2017**, *47*, 9−13.
(46) Wang, S. Y. W. L.; Lu, X. B.; Li, Q. P. Numerical Analysis of the Effects of Gas Hydrate Dissociation on the Stability of Deposits and Pipes. *China Offshore Oil Gas* **2008**, *20*, 6.

https://dx.doi.org/10.1021/acsomega.0c05463
ACS Omega 2021, 6, 5335−5347